



## Effect of a radiolabel biochemical nature on tumor-targeting properties of EpCAM-binding engineered scaffold protein DARPIn Ec1

Sergey M. Deyev<sup>a,b,c,1</sup>, Anzhelika Vorobyeva<sup>b,d,1</sup>, Alexey Schulga<sup>a,b</sup>, Ayman Abouzayed<sup>f</sup>, Tyran Günther<sup>d</sup>, Javad Garousi<sup>d</sup>, Elena Konovalova<sup>a</sup>, Haozhong Ding<sup>e</sup>, Torbjörn Gräslund<sup>e</sup>, Anna Orlova<sup>b,f,g</sup>, Vladimir Tolmachev<sup>b,d,\*</sup>

<sup>a</sup> Molecular Immunology Laboratory, Shemyakin & Ovchinnikov Institute of Bioorganic Chemistry, Russian Academy of Sciences, Moscow, Russia

<sup>b</sup> Research School of Chemistry and Applied Biomedical Sciences, Research Tomsk Polytechnic University, Tomsk, Russia

<sup>c</sup> Center of Biomedical Engineering, Sechenov University, Moscow, Russia

<sup>d</sup> Department of Immunology, Genetics and Pathology, Uppsala University, Uppsala, Sweden

<sup>e</sup> Department of Protein Science, KTH Royal Institute of Technology, Stockholm, Sweden

<sup>f</sup> Department of Medicinal Chemistry, Uppsala University, Uppsala, Sweden

<sup>g</sup> Science for Life Laboratory, Uppsala University, Uppsala, Sweden

### ARTICLE INFO

#### Article history:

Received 16 November 2019

Received in revised form 17 December 2019

Accepted 17 December 2019

Available online 19 December 2019

#### Keywords:

Designed ankyrin repeat protein

EpCAM

Labeling

Structure-property relationship

Biodistribution

### ABSTRACT

Radionuclide-based imaging of molecular therapeutic targets might facilitate stratifying patients for specific biotherapeutics. New type of imaging probes, based on designed ankyrin repeat proteins (DARPin), have demonstrated excellent contrast of imaging of human epidermal growth factor type 2 (HER2) expression in preclinical models. We hypothesized that labeling approaches, which result in lipophilic radiometabolites (non-residualizing labels), would provide the best imaging contrast for DARPins that internalize slowly after binding to cancer cells. The hypothesis was tested using DARPIn Ec1 that binds to epithelial cell adhesion molecule (EpCAM). EpCAM is a promising therapeutic target. Ec1 was labeled with <sup>125</sup>I using two methods to obtain the non-residualizing labels, while residualizing labels were obtained by labeling it with <sup>99m</sup>Tc. All labeled Ec1 variants preserved target specificity and picomolar binding affinity to EpCAM-expressing pancreatic adenocarcinoma BxPC-3 cells. In murine models, all the variants provided similar tumor uptake. However, <sup>125</sup>I-PIB-H<sub>6</sub>-Ec1 had noticeably lower retention in normal tissues, which provided appreciably higher tumor-to-organ ratios. Furthermore, <sup>125</sup>I-PIB-H<sub>6</sub>-Ec1 demonstrated the highest imaging contrast in preclinical models than any other EpCAM-imaging agent tested so far. In conclusion, DARPIn Ec1 in combination with a non-residualizing label is a promising probe for imaging EpCAM expression a few hours after injection.

### 1. Introduction

Biopharmaceuticals are the most commonly type of biological macromolecules used in medicine. Biopharmaceuticals, such as monoclonal antibodies and their derivatives, act specifically on malignant cells carrying a particular cancer-specific molecular abnormality (molecular target). This permits selective elimination of cancer cells but spares normal tissues, making these biopharmaceuticals attractive for treatment of disseminated malignancies. However, heterogeneity of molecular target expression is a serious issue in targeted cancer therapy [1]. Tumors without expression of a particular target would not respond to the specific treatment, but patients would be exposed to potential side effects.

A common practice (e.g. in selecting patients for HER2-targeting therapy) is to perform an analysis of the target expression using tumor biopsy material [2]. The major problem is the invasiveness of such procedures hampering multiple biopsies. This prevents addressing a discordance of a specific target's expression in synchronous metastases as well as the changing of target expression due to treatment.

In order to select potential responders, imaging of molecular target expression using positron emission tomography (PET) or single photon emission computed tomography (SPECT) could be performed before treatment. Unlike the biopsy-based methodology, this stratification approach is non-invasive, repetitive, and provides global information on target expression in vivo [3,4]. In daily clinical practice, such imaging would prevent overtreatment of patients with a too low target expression. Moreover, the selection of potential responders would contribute to the success of clinical trials for novel targeting biopharmaceuticals.

Several clinical trials have demonstrated the feasibility of imaging molecular targets using radiolabeled therapeutic monoclonal antibodies

\* Corresponding author at: Department of Immunology, Genetics and Pathology, Uppsala University, SE-75185 Uppsala, Sweden.

E-mail address: [vladimir.tolmachev@igp.uu.se](mailto:vladimir.tolmachev@igp.uu.se) (V. Tolmachev).

<sup>1</sup> Contributed equally.

[5–7]. The major hindrance in the use of antibodies for imaging is their large size (molecular weight of 150 kDa). This results in a slow tumor accumulation of the imaging probe and its slow clearance from the blood. Therefore, a reasonable imaging contrast might be obtained only several days after injection. In addition, nonspecific accumulation in tumors due to the “enhanced permeability and retention” (EPR) effect reduces the specificity of imaging.

A promising alternative to monoclonal antibodies and their derivatives would be the use of another type of biological macromolecules, engineered scaffold proteins (ESPs) as targeting probes [8]. The common feature of such proteins is the use of a robust framework, which in combination with molecular display enables selecting very high-affinity binders to different molecular targets [9,10]. The use of non-immunoglobulin scaffold proteins permits the creation of small (molecular weight in the range of 4–20 kDa) targeting probes with good extravasation properties and rapid tumor localization. Fast renal excretion of unbound probes facilitates a high imaging contrast just several hours after injection [8]. It has to be noted that the affinity of ESP binders to molecular targets depends on the spatial geometry of their binding surfaces. Therefore, some ESPs might fit better for the targeting of certain types of epitopes. Thus, a panel of different types of ESPs would be desirable for selecting the best imaging probe for each therapeutic target.

Designed ankyrin repeat proteins (DARPin)s are a type of ESP consisting of 4–6 repeat modules (each of 33 amino acids) and having a molecular weight of 14–18 kDa. DARPins with subnanomolar affinity for several molecular targets have been selected [10,11]. Pre-clinical evaluation of HER2-binding DARPins have previously demonstrated very good imaging properties of these ESPs [12–16]. Furthermore, a set of excellent technologies developed by the team of Prof. Plückthun has enabled the efficient selection of high-affinity DARPins binders to a variety of therapeutic targets [10]. This has created a precondition for the efficient development of novel probes providing high-contrast imaging. Another key factor during probe development is the labeling strategy (i.e. selection of an appropriate radionuclide and a linker or chelator for its coupling to a targeting protein).

Selecting a labeling strategy is relatively easy for monoclonal antibodies, since their biodistribution is not critically dependent on the labeling strategy, at least when a limited number of chelators per molecule is coupled [17,18]. Thus, the major criteria are sufficient half-life of the radionuclide, and the internalization pattern of the antibody after binding to the cancer cells. Since the bivalent binding of an antibody usually triggers internalization, trafficking to a lysosomal compartment and subsequent proteolysis, the preferable type of label would be a residualizing one, i.e. trapped intracellularly after proteolytic degradation (For explanation, see Fig. 1). Thus, the vast majority of antibodies developed for immunoPET imaging are labeled in the same way, i.e. by coupling of the chelator desferrioxamine (DFO) and a long-lived positron emitter  $^{89}\text{Zr}$  ( $T_{1/2} = 78.4$  h) [5–7,19].

Selecting the radiolabeling strategy for ESPs is more complicated, as these probes are much smaller and labeling changes their physicochemical properties to a high extent. Our experience with affibody molecules has demonstrated that the labeling strategy can influence an ESP's binding affinity to its molecular target, cellular processing and intracellular retention of radiometabolites in malignant cells after internalization, as well as its off-target interaction with normal tissues. The predominant excretion pathway of the imaging probe, its uptake and retention in excretory organs and the excretion of its radiometabolites may be affected as well [20]. This all influences the imaging contrast and therefore its sensitivity. In pursuit of the highest possible sensitivity, we have evaluated the influence of eleven different nuclides and more than one hundred combinations of a nuclide and a chelator/linker on the imaging properties of affibody molecules. This finally resulted in a several-fold increase in the imaging contrast, but took several years to achieve. It would be desirable to develop generalizable approaches to the labeling

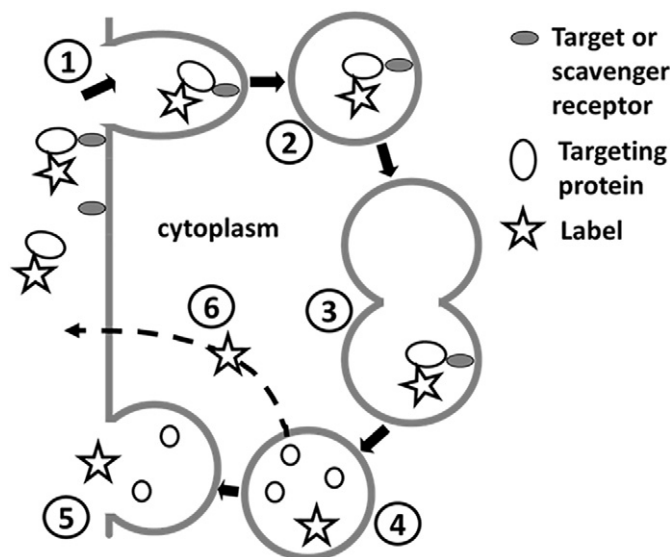


**Fig. 1.** Cellular processing of radiolabeled protein after binding to a cell-associated target or scavenger receptor. After binding to a molecular target (on cancer cells or normal tissues) or a scavenger receptor (in proximal tubuli of kidneys) a radiolabeled targeting protein undergoes an internalization (1). The internalized protein is transferred to endosomal (2) and then lysosomal compartment (3). In lysosomal compartment, the protein is undergoing a proteolytic degradation (4). If radiometabolites are charged or bulky polar moieties, they are excreted by slow externalization process (5). Labels that are metabolized in this way are called *residualizing labels*. If radiometabolites are lipophilic, they can diffuse through lysosomal and cellular membranes (6) and rapidly “leak” from cells. Such kind of labels are called *non-residualizing labels*.

chemistry thus permitting development of new ESP-based probes providing high imaging contrast in a more expeditious manner.

The major findings during the development of HER2-imaging DARPins probes could be summarized as follows: presence of the hexahistidine tag resulted in an elevated hepatic uptake of DARPins when labeled using residualizing radiometals; substitution of the hexahistidine tag by a histidine-glutamate-histidine-glutamate-histidine-glutamate (HEHEHE- or  $(\text{HE})_3$ ) tag resulted in a three-fold decrease in hepatic uptake [12,16]; use of residualizing  $^{99\text{m}}\text{Tc}(\text{CO})_3\text{-H}_6\text{-}$ ,  $^{99\text{m}}\text{Tc}(\text{CO})_3\text{-(HE)}_3\text{-}$  or  $^{111}\text{In-DOTA}$ -labels resulted in long retention in both tumors and normal tissues [12,14,16]; internalization of anti-HER2 DARPins after binding to HER2 expressing cells was slow. Therefore, the use of non-residualizing radioiodine labels did not reduce the tumor uptake in comparison with residualizing labels, especially when imaging (or ex vivo measurement) was performed several hours after injection [14]. However, the use of non-residualizing radioiodine labels resulted in a very significant reduction of uptake in normal tissues, first and foremost in the liver and kidneys, where DARPins are apparently internalized [13–15,21]. Thus, the use of a non-residualizing label provided better imaging contrast for HER2-targeted DARPins. It should be noted, that directly translating findings made for one DARPins-based probe to another may be overly optimistic because different DARPins might differ appreciably from each other. DARPins may contain a different number of repeats. Moreover, target-specific selection results in a very different composition of the binding amino acids, which constitute a substantial fraction of the solvent-exposed surface. It has also been observed that substitution of only three amino acids in G3 DARPins resulted in a noticeable difference in biodistribution [16]. This makes it necessary to test whether the same labeling approach would have a similar effect on other DARPins.

DARPins Ec1, which binds to epithelial cell adhesion molecule (EpcAM) with very high affinity (68 pM), was used as a model to test the influence of different labeling approaches [22]. The specificity of Ec1 binding to EpcAM has been demonstrated previously by several orthogonal methods [22]. EpcAM (other designations: DIAR5, EGP-2, EGP314, EGP40, ESA, HNPCC8, KS1/4, KSA, M4S1, MIC18, MK-1,

TACSTD1, TROP1) is an actively investigated therapeutic target in several types of cancer, such as pancreatic adenocarcinoma, ovarian and breast cancers. Several anti-EpCAM monoclonal antibodies and antibody-based constructs are under clinical evaluation [23]. EpCAM is a known biomarker of circulating tumor cells and cancer stem cells [24]. Our particular selection of DARPIn Ec1 for labeling was based on the consideration that it might be useful for stratification of pancreatic cancer patients awaiting EpCAM-targeted therapy. Disseminated pancreatic cancer is a disease which is difficult to treat [25,26]. In pancreatic cancer, EpCAM overexpression (intense grade) is found in 23–37% of patients (depending on the threshold applied) [27,28]. EpCAM-positive pancreatic cancer stem cells have a 100-fold higher tumorigenic potential than EpCAM-negative cells [29], which further supports the development of anti-EpCAM therapies for preventing cancer progression. However, there is an inter-tumoral and inter-patient heterogeneity of EpCAM overexpression [28,30]. Apparently, only tumors with a high level of EpCAM overexpression respond to EpCAM-directed treatment [30]. Therefore, we selected pancreatic cancer BxPC-3 cells as a primary model in our study.

Two variants of Ec1, one with a hexahistidine tag and one with a (HE)<sub>3</sub>-tag, were produced and designated H<sub>6</sub>-Ec1 and (HE)<sub>3</sub>-Ec1 respectively (Supplementary Fig. S1). To evaluate the use of non-residualizing labels, H<sub>6</sub>-Ec1 was labeled directly with <sup>125</sup>I (using Chloramine-T) and indirectly using <sup>125</sup>I-N-succinimidyl-4-iodobenzoate (Supplementary Fig. S2A and B). To evaluate the use of residualizing labels, H<sub>6</sub>-Ec1 and (HE)<sub>3</sub>-Ec1 were labeled with <sup>99m</sup>Tc(CO)<sub>3</sub> (Supplementary Fig. S2C and S2D). These labels were selected because the residualizing properties of <sup>99m</sup>Tc(CO)<sub>3</sub> have been demonstrated for a variety of targeting proteins in multiple papers in combination with H<sub>6</sub>- and (HE)<sub>3</sub>- (see e.g. [31–36]) tags. This is manifested as a strong retention of activity after reabsorption and internalization in the kidneys (as strong as in the case of <sup>111</sup>In or <sup>177</sup>Lu). The non-residualizing properties of the direct iodine label and iodobenzoate label are also well known (see e.g. [36–38]). Binding specificity, affinity and cellular processing of all variants were evaluated *in vitro* using the EpCAM-expressing BxPC-3 pancreatic cancer cell line. A comparison of the biodistribution for all variants was performed in mice bearing BxPC-3 xenografts. The most promising variant, <sup>125</sup>I-PIB-H<sub>6</sub>-Ec1, was further characterized using biodistribution and imaging experiments.

## 2. Materials and methods

### 2.1. Production, characterization and radiolabeling of DARPins

H<sub>6</sub>-Ec1 (containing a hexahistidine tag) and (HE)<sub>3</sub>-Ec1 (containing a HEHEHE tag) were produced based on sequences published by Stefan et al. [22] using methodology described earlier for anti-HER2 DARPins [14]. Purification was performed using a combination of immobilized metal ion chromatography (IMAC) and ion-exchange chromatography [14]. The purity and authenticity of the purified proteins were analyzed by liquid chromatography electrospray ionization mass spectrometry (LC-ESI-MS) on a 6520 Accurate Q-TOF LC-MS (Agilent).

Direct radioiodination of H<sub>6</sub>-Ec1 and labeling of H<sub>6</sub>-Ec1 and (HE)<sub>3</sub>-Ec1 using <sup>99m</sup>Tc(CO)<sub>3</sub> was performed as described by Deyev and co-workers [14]. Indirect radioiodination using N-succinimidyl-para-(trimethylstannyl)benzoate was performed as described earlier for antibody molecules [39]. All labeled proteins were purified using NAP-5 size-exclusion columns (GE Healthcare, Sweden). The identity and purity of radiolabeled DARPins was confirmed using HPLC. Radio-high performance liquid chromatography (HPLC) analysis was performed using a Hitachi Chromaster HPLC system with a radioactivity detector and Vydac RP C18 column (300 Å; 3 × 150 mm; 5-μm) at room temperature (20 °C). The sample quantity used for analysis was 5 μl. Solvent A was 0.1% trifluoroacetic acid (TFA) in H<sub>2</sub>O; solvent B was 0.1% TFA in acetonitrile. The flow rate was 1 ml/min, with a 5% B to 80% B gradient over 20 min. The stability of <sup>125</sup>I- and <sup>99m</sup>Tc-labels was assessed by using

challenge reactions containing a large excess of either stable iodide or histidine, respectively, as described by Vorobyeva and co-workers [13].

### 2.2. Characterization of radiolabeled DARPins *in vitro*

Binding specificity and cellular processing of radiolabeled DARPins were evaluated using EpCAM-expressing BxPC-3 and Panc-1 pancreatic cancer cells (ATCC) by the method described for anti-HER2 DARPins [14]. For the specificity test, cells were incubated with 2 nM (equivalent to ca. 25-fold the K<sub>D</sub> value) of radiolabeled conjugate and the cell-associated activity was measured. Cells, pre-incubated with unlabeled Ec1 (100-fold molar excess), were used as a control.

To evaluate the internalization by cancer cells after binding, BxPC-3 cells were incubated with the labeled DARPins (1 nM) at 37 °C. Discrimination between membrane-bound and internalized activity was determined using a modified acid wash method [40]. The maximum value of cell-bound activity in each dataset was taken as 100% and the data were normalized to that value.

Binding affinities of the radiolabeled DARPins to living BxPC-3 cells were measured using the LigandTracer instrument (Ridgeview Instruments, Vänge, Sweden) and evaluated using TraceDrawer Software (Ridgeview Instruments AB, Vänge, Sweden) according to the method described earlier [41]. Briefly, increasing concentrations of radiolabeled DARPins were added to the cells to record the binding kinetics. Thereafter, the cell media was replaced and the retention in the dissociation phase was measured. Binding and dissociation kinetics was recorded at room temperature.

### 2.3. Animal studies

Animal studies were performed in agreement with Swedish national legislation concerning protection of laboratory animals and were approved by the Ethics Committee for Animal Research in Uppsala (ethical permission C5/16 from 26-02-2016).

To select an optimal label, the biodistribution of <sup>125</sup>I-PIB-H<sub>6</sub>-Ec1, <sup>125</sup>I-H<sub>6</sub>-Ec1, <sup>99m</sup>Tc(CO)<sub>3</sub>-H<sub>6</sub>-Ec1 and <sup>99m</sup>Tc(CO)<sub>3</sub>-(HE)<sub>3</sub>-Ec1 was evaluated in BALB/C nu/nu mice bearing BxPC-3 xenografts 3 h post-injection (pi). To establish BxPC-3 xenografts, 10<sup>7</sup> cells were implanted subcutaneously in 8-week old mice. For a specificity control, 10<sup>7</sup> of EpCAM-negative Ramos cells were implanted. As HT-29 colorectal cancer is a commonly used model in EpCAM studies, the biodistribution of the most promising Ec1 variant <sup>125</sup>I-PIB-H<sub>6</sub>-Ec1 was evaluated in mice bearing HT-29 tumors at 3 h pi as well. For this purpose, 5 × 10<sup>6</sup> HT-29 cells were implanted subcutaneously in 8-week old mice. At the time of experimentation (two to three weeks after implantation) the weights of the animals were 18 ± 2 g. Average tumor weights were 0.56 ± 0.2 g for BxPC-3, 0.3 ± 0.2 g for Ramos and 0.6 ± 0.2 g for HT-29. Groups of four to eight animals per data point were used.

To select an optimal label, mice were injected with: <sup>125</sup>I-PIB-H<sub>6</sub>-Ec1 and <sup>125</sup>I-H<sub>6</sub>-Ec1 (both non-residualizing labels), <sup>99m</sup>Tc(CO)<sub>3</sub>-H<sub>6</sub>-Ec1 and <sup>99m</sup>Tc(CO)<sub>3</sub>-(HE)<sub>3</sub>-Ec1 (both residualizing labels) and the biodistribution was measured 3 h pi. The injected activity was 30 kBq/mouse for <sup>99m</sup>Tc and 20 kBq/mouse for <sup>125</sup>I. The injected protein dose was adjusted to 4 μg/mouse using unlabeled protein. The labeled proteins were injected into a tail vein. The mice were anesthetized by an intraperitoneal injection of a ketamine HCl (Ketalar, Pfizer) and xylazine HCl (Rompun; Bayer) mixture (20 μl of solution per gram of body weight; Ketalar 10 mg/ml, Rompun 1 mg/ml) and exsanguinated by a syringe rinsed with diluted heparin (Leo Pharma). Blood and organ samples were collected, weighed and their activity was measured using an automated gamma-spectrometer with a NaI(Tl) detector (1480 Wizard, PerkinElmer). The <sup>125</sup>I activity was measured in the energy window from 4 to 80 keV, and <sup>99m</sup>Tc was measured from 100 to 200 keV. Organ uptake values were calculated as percent injected dose per gram tissue (% ID/g) except for the intestines, which were measured as whole sample.

For the most promising variant,  $^{125}\text{I}$ -PIB- $\text{H}_6$ -Ec1, the biodistribution was additionally measured in mice bearing BxPC-3 tumors at 6 h pi, as described above. To confirm specificity, the uptake of  $^{125}\text{I}$ -PIB- $\text{H}_6$ -Ec1 was measured in EpCAM-negative Ramos lymphoma xenografts at 6 h pi. In addition, an *in vivo* saturation experiment was performed. EpCAM in BxPC-3 xenografts was saturated by subcutaneous injection of unlabeled protein at 1.5 mg/mouse 60 min before injection of  $^{125}\text{I}$ -PIB- $\text{H}_6$ -Ec1, and tumor uptake was measured at 6 h pi. Biodistribution of  $^{125}\text{I}$ -PIB- $\text{H}_6$ -Ec1 was also measured in BALB/C nu/nu mice bearing HT-29 xenografts 3 h after injection.

Whole body SPECT/CT scans of mice bearing BxPC-3 tumors and injected with  $^{125}\text{I}$ -PIB- $\text{H}_6$ -Ec1 (6  $\mu\text{g}$ , 0.35 MBq) or with  $^{125}\text{I}$ - $\text{H}_6$ -Ec1 (6  $\mu\text{g}$ , 2.5 MBq) were performed using nanoScan SPECT/CT (Mediso Medical Imaging Systems, Hungary). Imaging at 6 h pi was performed after mice were sacrificed by  $\text{CO}_2$  inhalation. The acquisition time was 20 min. CT scans were acquired using the following parameters: X-ray energy peak of 50 keV; 670  $\mu\text{A}$ ; 480 projections; and 5.26 min acquisition time. SPECT raw data were reconstructed using Tera-Tomo™ 3D SPECT reconstruction technology (version 3.00.020.000; Mediso Medical Imaging Systems Ltd.): normal dynamic range; 30 iterations; and one subset. CT data were reconstructed using Filter Back Projection in Nucline 2.03 Software (Mediso Medical Imaging Systems Ltd.). SPECT and CT files were fused using Nucline 2.03 Software and are presented as maximum intensity projections in the RGB color scale.

#### 2.4. Statistical analysis

Statistical analysis was performed using Prism 8.1.1 software (GraphPad Software Inc). A 2-tailed unpaired *t*-test was applied to find a significant difference for comparison of two sets of data. For comparison of more than two sets of data, a 1-way ANOVA with Bonferroni multiple comparisons post-hoc test was used.

### 3. Results

#### 3.1. Ec1 production and labeling

Two constructs,  $\text{H}_6$ -Ec1 and  $(\text{HE})_3$ -Ec1, were produced in *E. coli* and purified using IMAC followed by ion-exchange chromatography. The authenticity of the conjugates was confirmed by LC-ESI-MS, which demonstrated excellent agreement between calculated and found molecular weights (Fig. 2). For  $\text{H}_6$ -Ec1, the calculated molecular weight was 18,349 and the found molecular weight was 18,348, and for  $(\text{HE})_3$ -Ec1, the calculated molecular weight was 17,980 and the found molecular weight was 17,980. The difference between calculated and found molecular weight was thus 1 and 0 Da, respectively. The purity of both variants was over 95%.

Characteristics of the labeling procedures and labeled DARPins are presented in Table 1. Size-exclusion chromatography provided radiochemical purities over 98%. All labels were stable under the challenge reaction conditions (i.e. no measurable release of radionuclides from their conjugates).

**Table 1**  
Characteristics of radiolabeled Ec1 variants.

	Radiochemical yield (%)	Radiochemical purity (%)	Binding affinity to BxPC-3 cells ( $K_D$ , pM)
$^{125}\text{I}$ - $\text{H}_6$ -Ec1	96 $\pm$ 2	99 $\pm$ 1	39 $\pm$ 3 (n = 2)
$^{125}\text{I}$ -PIB- $\text{H}_6$ -Ec1	23 $\pm$ 2	99 $\pm$ 0	58 $\pm$ 13 (n = 3)
$^{99\text{m}}\text{Tc}(\text{CO})_3$ - $\text{H}_6$ -Ec1	89 $\pm$ 3	99 $\pm$ 1	51 $\pm$ 4 (n = 2)
$^{99\text{m}}\text{Tc}(\text{CO})_3$ - $(\text{HE})_3$ -Ec1	81 $\pm$ 8	98 $\pm$ 1	88 $\pm$ 13 (n = 2)

#### 3.2. Characterization of radiolabeled DARPins *in vitro*

Results from the blocking test demonstrated that pre-treatment of BxPC-3 and Panc-1 cells with a large excess of unlabeled Ec1 caused a highly significant ( $p < 0.00005$ ) reduction in binding of the radiolabeled DARPins. This demonstrated a saturable hence specific character of binding. The cell-bound activity values were similar for all variants and were higher for BxPC-3 cells compared to Panc-1, reflecting their higher EpCAM expression levels [42] (Supplementary Fig. S3).

LigandTracer measurements (Table 1) demonstrated that all radiolabeled Ec1 variants had a picomolar affinity, indicating very little influence of the labeling approaches on their binding.

Data concerning the cellular processing of radiolabeled DARPins are presented in Fig. 3. A characteristic feature of radiolabeled Ec1 was slow internalization (ca. 25% was internalized after 24 h incubation). Both the total cell-associated and internalized activity increased continuously for the technetium-labeled variants while there was a plateau between 6 and 24 h for the radioiodinated DARPins. This plateau could be explained by the non-residualizing properties of the iodine labels and the consequent diffusion of iodine catabolites out of the cells after internalization.

#### 3.3. *In vivo* studies

Data concerning the biodistribution of radiolabeled Ec1 variants in mice, bearing BxPC-3 xenografts 3 h post-injection (pi), are presented in Fig. 4A. Rapid blood clearance was characteristic for all variants. Low radioactivity in the gastrointestinal tract (with contents) and high kidney retention of the residualizing labels suggested a renal excretion pathway. Tumor uptake for all variants did not differ significantly. However, there were noticeable significant differences ( $p < 0.05$ ) in their distribution throughout normal tissues. The renal uptake of  $^{99\text{m}}\text{Tc}$ -labeled DARPins was >20-fold higher compared to their radioiodinated counterparts.  $^{99\text{m}}\text{Tc}(\text{CO})_3$ - $\text{H}_6$ -Ec1 had the highest uptake in the liver and spleen. Use of the HEHEHE tag for labeling with  $^{99\text{m}}\text{Tc}$  resulted in a significantly reduced uptake in the liver, spleen, pancreas and stomach compared with  $^{99\text{m}}\text{Tc}(\text{CO})_3$ - $\text{H}_6$ -Ec1. Despite this, the hepatic uptake of  $^{99\text{m}}\text{Tc}(\text{CO})_3$ - $(\text{HE})_3$ -Ec1 was still higher than the tumor uptake. The radioiodinated DARPins had appreciably lower hepatic and renal uptakes. However, there was obvious evidence of the redistribution of radiometabolites for the direct iodine label, e.g. elevated activity in the

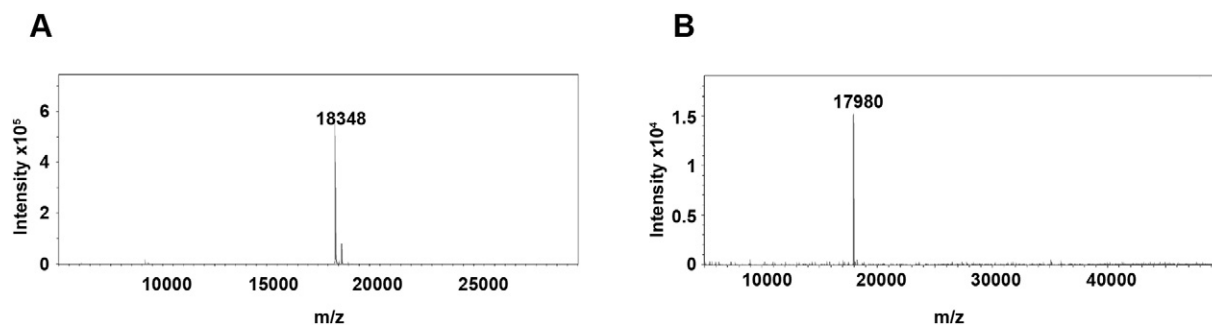


**Fig. 2.** Deconvolution results from mass-spectrometry of  $\text{H}_6$ -Ec1 (A) and  $(\text{HE})_3$ -Ec1 (B).

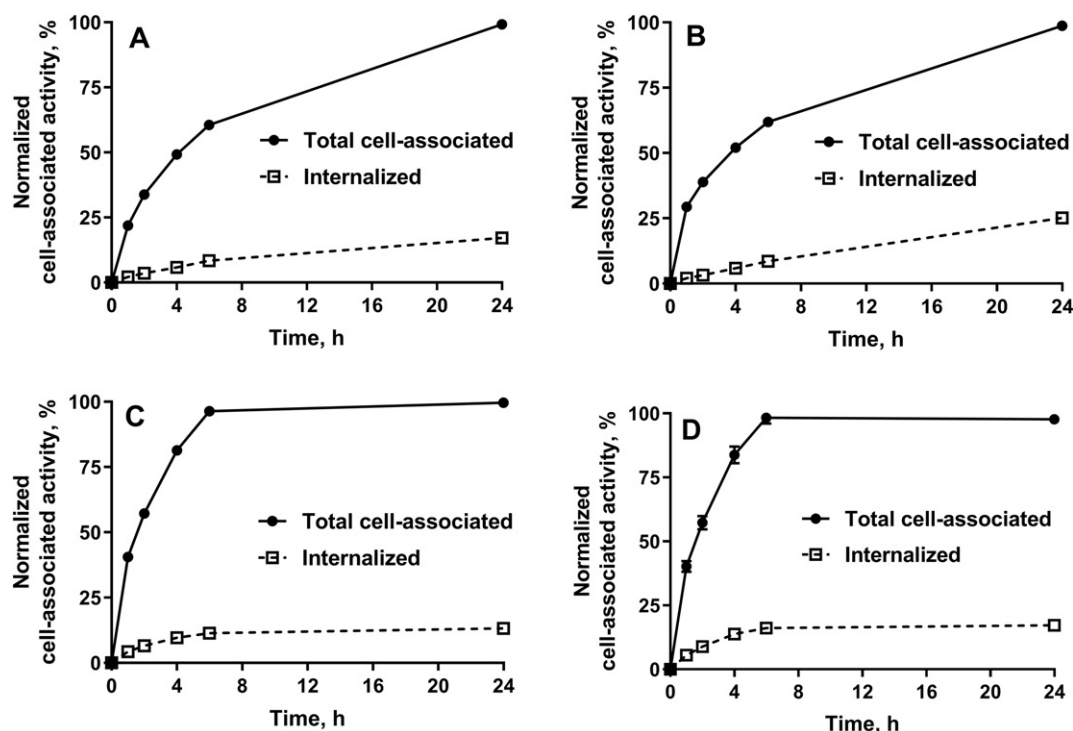


**Fig. 3.** Cellular processing of: (A)  $^{99m}\text{Tc}(\text{CO})_3\text{-H}_6\text{-Ec1}$ ; (B)  $^{99m}\text{Tc}(\text{CO})_3\text{-(HE)}_3\text{-Ec1}$ ; (C)  $^{125}\text{I-H}_6\text{-Ec1}$ ; (D)  $^{125}\text{I-PIB-H}_6\text{-Ec1}$  by BxPC-3 cells. Cells were incubated with the conjugates (1 nM) at 37 °C. Data are presented as the mean of three samples  $\pm$  standard deviation (SD). Error bars might not be seen when they are smaller than data point symbols.

blood, salivary gland, stomach and gastrointestinal tract. Overall,  $^{125}\text{I-PIB-H}_6\text{-Ec1}$  had the lowest uptake in normal tissues. Accordingly,  $^{125}\text{I-PIB-H}_6\text{-Ec1}$  provided significantly higher tumor-to-organ ratios compared to the other radiolabeled Ec1 variants (Fig. 4B). The only exceptions were the tumor-to-lung (no significant difference with  $^{99m}\text{Tc}(\text{CO})_3\text{-(HE)}_3\text{-Ec1}$ ) and tumor-to-kidney ratios (significantly higher for  $^{125}\text{I-H}_6\text{-Ec1}$ ).

Regarding  $^{125}\text{I-PIB-H}_6\text{-Ec1}$ , increasing the time between injection and biodistribution measurements to 6 h resulted in a significant ( $p < 0.05$ ) decrease in activity in all organs and tissues (except the rest of the GI tract) but not in tumors (Table 2). This resulted in a significant increase in all tumor-to-organ ratios (except the tumor-to-intestine ratio) at the later time point (Table 3).

The results of the specificity test (Fig. 5) demonstrated that uptake of  $^{125}\text{I-PIB-H}_6\text{-Ec1}$  in EpCAM-negative Ramos xenografts was much lower ( $p < 0.0005$ ) than in EpCAM-positive BxPC-3 xenografts. In addition, saturation of EpCAM by pre-injecting unlabeled Ec1 resulted in a significant ( $p < 0.0005$ ) reduction in tumor uptake.

SPECT/CT imaging demonstrated that  $^{125}\text{I-PIB-H}_6\text{-Ec1}$  provided high contrast imaging of BxPC-3 xenografts (Fig. 6A). Besides tumors, only the kidneys demonstrated a noticeable activity uptake. By comparison,  $^{125}\text{I-H}_6\text{-Ec1}$  (Fig. 6B) had lower renal uptake than  $^{125}\text{I-PIB-H}_6\text{-Ec1}$ , but higher uptake in other abdominal organs and tissues, especially the stomach.

Since a number of reported EpCAM imaging probes were evaluated using HT-29 colorectal cancer xenografts [43,44], we performed biodistribution studies of  $^{125}\text{I-PIB-H}_6\text{-Ec1}$  in mice bearing HT-29 tumors at 3 h after injection (Table 4). The overall pattern of biodistribution was similar to the BxPC-3 model at 3 h pi, with somewhat higher activity in the blood, salivary glands, stomach, pancreas, small intestine and muscles ( $p < 0.05$ ). The uptake of  $^{125}\text{I-PIB-H}_6\text{-Ec1}$  in HT-29 tumors was at the same level as the uptake in BxPC-3 tumors ( $3.2 \pm 0.6$  vs.  $3.8 \pm 0.9\%$  ID/g;  $p > 0.05$ ). In this model  $^{125}\text{I-PIB-H}_6\text{-Ec1}$  provided tumor-to-blood ratio of  $10 \pm 1$ , tumor-to-liver ratio of  $12 \pm 1$ , and tumor-to-muscle ratio of  $26 \pm 5$  at 3 h pi.

#### 4. Discussion

This study has demonstrated that DARPIn Ec1 can be labeled using several approaches and still preserve its specificity (Fig. S3) and affinity (Table 1) of binding to EpCAM-expressing cells in vitro. Importantly, the internalization of radiolabeled Ec1 by cancer cells was slow (Fig. 2). This suggested that the residualizing properties of the label might not be critical for good retention of the activity in tumors. Instead, the preservation of high affinity was considered more important. On the other hand, a typical feature of non-residualizing labels is that they could facilitate a rapid release of activity from organs and tissues where the probe could have been internalized due to off-target interactions. Indeed, the tumor uptakes for all the tested radiolabeled variants did not differ significantly at 3 h after injection, but there was a striking difference in normal organ uptakes (Fig. 4A). The most prominent difference was in renal uptake, where both  $^{99m}\text{Tc}(\text{CO})_3\text{-H}_6\text{-Ec1}$  and  $^{99m}\text{Tc}(\text{CO})_3\text{-(HE)}_3\text{-Ec1}$  demonstrated a high retention of activity while activities from  $^{125}\text{I-PIB-H}_6\text{-Ec1}$  and  $^{125}\text{I-H}_6\text{-Ec1}$  (both with non-residualizing labels) were rapidly released. Another important example was the hepatic uptake, as the liver is the main metastatic site for many malignancies [45]. The hepatic uptake of  $^{99m}\text{Tc}(\text{CO})_3\text{-H}_6\text{-Ec1}$  was high ( $12.9 \pm 0.6\%$  ID/g), which was similar to the HER2-targeting DARPIn 9\_29 labeled using the same method [13,14].

Experience with other ESPs, affibody molecules, showed that replacement of the hexahistidine tag with the more hydrophilic negatively charged HEHEHE-tag reduced uptake in the liver ten-fold when labeled with  $^{99m}\text{Tc}(\text{CO})_3$  [46,47]. However, the use of this tag did not reduce the hepatic uptake of an ADAPT ESP which was similarly labeled with  $^{99m}\text{Tc}(\text{CO})_3$  [48]. Thus, it cannot be generalized that the HEHEHE-tag has the same effect on biodistribution for all ESPs. The use of this tag for labeling Ec1 reduced the hepatic uptake 2.3-fold (Fig. 4A). This is in agreement with the data for the anti-HER2 DARPIn G3 [16], where the hepatic uptake was reduced 3-fold. This indicates that similar effects of the HEHEHE-tag might be expected for other DARPIns, independent of their binding sites. However, the hepatic uptake of  $^{99m}\text{Tc}$

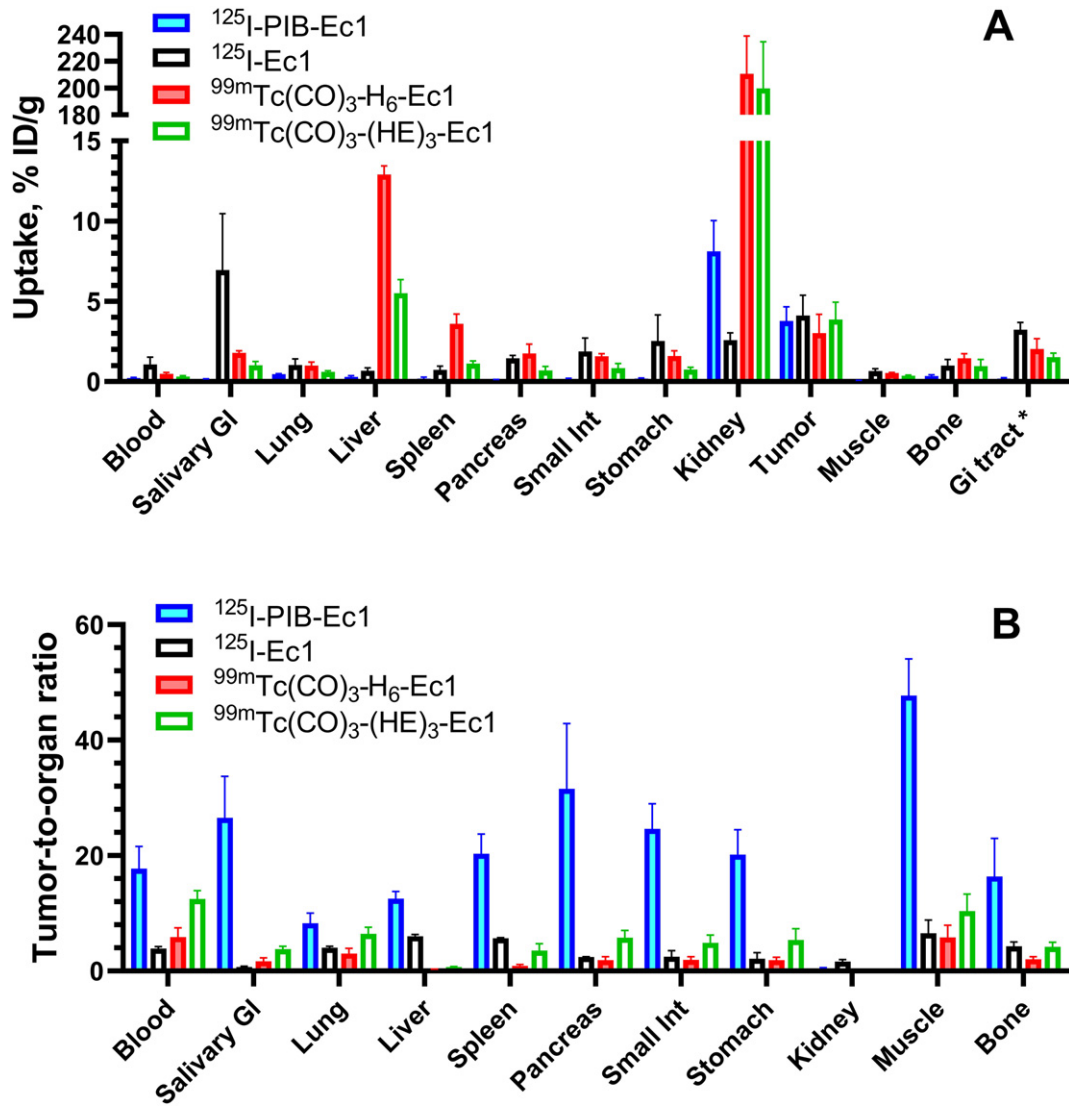


**Fig. 4.** Biodistribution (A) and tumor-to-organ ratios (B) of  $^{125}\text{I-PIB-H}_6\text{-Ec1}$ ,  $^{125}\text{I-H}_6\text{-Ec1}$ ,  $^{99\text{mTc(CO)}_3\text{-H}_6\text{-Ec1}$  and  $^{99\text{mTc(CO)}_3\text{-(HE)}_3\text{-Ec1}$  in BALB/C nu/nu mice bearing BxPC-3 xenografts 3 h after injection. Data are presented as mean  $\pm$  SD for four mice. \*Data for the gastrointestinal tract with content are presented as %ID per whole sample.

(CO)<sub>3</sub>-(HE)<sub>3</sub>-Ec1 was still higher than the tumor uptake, which reduces the value of this probe for cancer imaging.

The non-residualizing radioiodine labels provided appreciably lower uptake in both the kidneys and liver (Fig. 4A). However, redistribution

of radiometabolites of  $^{125}\text{I-H}_6\text{-Ec1}$  still resulted in elevated activity uptake in a number of tissues, first and foremost, in the salivary gland and stomach. Labeling Ec1 by conjugation with  $^{125}\text{I-N-succinimidy-para-iodobenzoate}$  resulted in the rapid excretion of radiometabolites, enabling a high ratio between activity concentration in the tumor and major metastatic sites for pancreatic cancer (the liver, lung and

**Table 2**

Biodistribution of  $^{125}\text{I-PIB-H}_6\text{-Ec1}$  in BALB/C nu/nu mice bearing BxPC-3 xenografts 3 and 6 h after injection. Data are presented as mean %ID/g  $\pm$  SD for four-eight mice. Data for the rest of the GI tract with contents are presented as %ID per whole sample.

	3 h	6 h
Blood	0.22 $\pm$ 0.05*	0.07 $\pm$ 0.01
Salivary gland	0.15 $\pm$ 0.03*	0.05 $\pm$ 0.01
Lung	0.46 $\pm$ 0.04*	0.16 $\pm$ 0.01
Liver	0.30 $\pm$ 0.07*	0.075 $\pm$ 0.008
Spleen	0.20 $\pm$ 0.08*	0.06 $\pm$ 0.01
Pancreas	0.12 $\pm$ 0.02*	0.03 $\pm$ 0.01
Small intestines	0.16 $\pm$ 0.06*	0.07 $\pm$ 0.02
Stomach	0.19 $\pm$ 0.03*	0.05 $\pm$ 0.02
Kidney	8 $\pm$ 2*	1.6 $\pm$ 0.4
Tumor	3.8 $\pm$ 0.9	3.2 $\pm$ 0.8
Muscle	0.08 $\pm$ 0.01*	0.026 $\pm$ 0.004
Bone	0.35 $\pm$ 0.08*	0.24 $\pm$ 0.05
Rest of GI tract	0.19 $\pm$ 0.05	0.25 $\pm$ 0.09

\* Significant difference ( $p < 0.05$ ) between uptake at 3 and 6 h after injection.

**Table 3**

Tumor-to-organ ratios of  $^{125}\text{I-PIB-H}_6\text{-Ec1}$  in BALB/C nu/nu mice bearing BxPC-3 xenografts at 3 and 6 h after injection. Data are presented as mean  $\pm$  SD for four-eight mice.

	3 h	6 h
Blood	18 $\pm$ 4*	50 $\pm$ 17
Salivary gland	26 $\pm$ 7*	62 $\pm$ 21
Lung	8 $\pm$ 2*	20 $\pm$ 5
Liver	13 $\pm$ 1*	43 $\pm$ 12
Spleen	20 $\pm$ 3*	55 $\pm$ 21
Pancreas	32 $\pm$ 11*	99 $\pm$ 40
Small intestines	25 $\pm$ 4*	46 $\pm$ 8
Stomach	20 $\pm$ 4*	65 $\pm$ 24
Kidney	0.5 $\pm$ 0.1*	2.1 $\pm$ 0.5
Muscle	48 $\pm$ 6*	126 $\pm$ 29
Bone	10.8 $\pm$ 0.8*	14 $\pm$ 2
Blood	18 $\pm$ 4*	50 $\pm$ 17

\* Significant difference ( $p < 0.05$ ) between uptake at 3 and 6 h after injection.

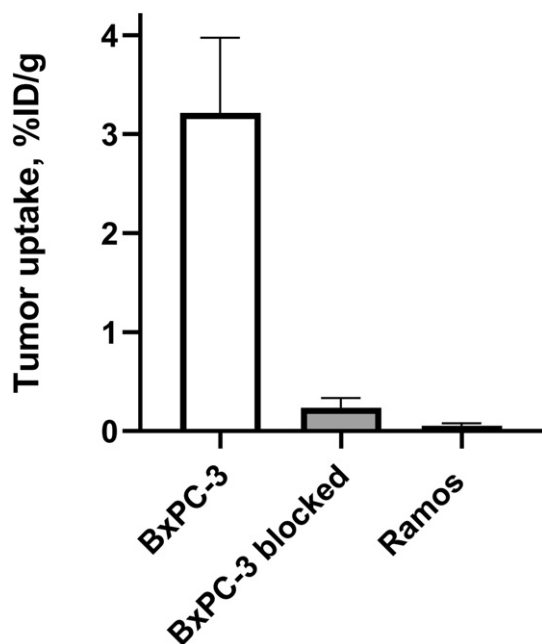


**Fig. 5.** In vivo specificity of EpCAM targeting using  $^{125}\text{I}$ -PIB-H<sub>6</sub>-Ec1. Uptake was significantly ( $p < 0.00005$ ) higher in EpCAM-positive BxPC-3 xenografts than in either EpCAM-negative Ramos or blocked BxPC-3 xenografts. EpCAM blocking was done by pre-injecting a large excess of unlabeled Ec1. Data are presented as mean  $\pm$  SD for four to eight mice.

abdominal organs [49]). For  $^{125}\text{I}$ -PIB-H<sub>6</sub>-Ec1, tumor-to-blood ratios of  $18 \pm 4$  and tumor-to-pancreas ratios of  $32 \pm 11$  were achieved already at 3 h after injection (Table 3). The tumor uptake did not decrease by 6 h, while uptake in normal tissues decreased further (Table 2). This resulted in a noticeable increase in tumor-to-organ ratios. For example, the tumor-to-blood ratio increased to  $58 \pm 19$  and the tumor-to-pancreas ratio to  $99 \pm 40$ . The data from this study are in good agreement with data for HER2-targeting DARPins [21] despite the structural differences in the DARPIn variants. Overall, our studies demonstrated that the influence of label types on biodistribution is similar for different

**Table 4**

Biodistribution and tumor-to-organ ratios of  $^{125}\text{I}$ -PIB-H<sub>6</sub>-Ec1 in BALB/C nu/nu mice bearing HT-29 xenografts 3 h after injection. Data are presented as mean %ID/g  $\pm$  SD for five mice.

	Uptake, %ID/g	T/O ratio
Blood	$0.32 \pm 0.06$	$10 \pm 1$
Salivary gland	$0.3 \pm 0.1$	$10 \pm 3$
Lung	$0.53 \pm 0.07$	$6 \pm 1$
Liver	$0.27 \pm 0.03$	$12 \pm 1$
Spleen	$0.19 \pm 0.03$	$17 \pm 3$
Pancreas	$0.26 \pm 0.07$	$13 \pm 5$
Small intestines	$0.3 \pm 0.07$	$12 \pm 5$
Stomach	$0.4 \pm 0.1$	$8 \pm 2$
Kidney	$5 \pm 1$	$0.7 \pm 0.3$
Tumor	$3.2 \pm 0.6$	–
Muscle	$0.13 \pm 0.02$	$26 \pm 5$
Bone	$0.3 \pm 0.05$	$11 \pm 2$

DARPins, which should streamline a process of development of DARPIn-based imaging probes.

The uptake of  $^{125}\text{I}$ -PIB-H<sub>6</sub>-Ec1 in human pancreatic cancer xenografts in mice is around 3.2%ID/g (Tables 2 and 4).  $^{111}\text{In}$ -DTPA-octreotide ( $^{111}\text{In}$ -Octreoscan) has been used for routine clinical imaging of neuroendocrine tumors since the mid-90s. Apparently, the tumor uptake of this tracer is sufficient for clinical use. The tumor uptake of  $^{111}\text{In}$ -DTPA-octreotide in a murine model is  $4.2 \pm 1.0\%$ ID/g (AR42J xenografts, 4 h after injection) [50],  $2.5 \pm 0.2\%$ ID/g (in NCI-H69 xenografts 4 h after injection) [51] and  $3.9 \pm 1.0\%$  ID/g (in AR42J xenografts, 3 h after injection) [52]. Thus, both the absolute uptake values and tumor-to-organ ratios provided by  $^{125}\text{I}$ -PIB-H<sub>6</sub>-Ec1 are sufficient to start a clinical translation.

Several probes for EpCAM visualization have been evaluated previously. In the 1990s, the pan-carcinoma expression of EpCAM motivated the development of radiolabeled monoclonal antibodies and their fragments for cancer staging. A radiolabeled murine monoclonal antibody  $^{111}\text{In}$ -DTPA-MOC-31 was evaluated for imaging of small-cell lung cancer [53]. Primary tumors or metastases were visualized in five out of six patients at 48 to 72 h after injection. An obvious issue with  $^{111}\text{In}$ -DTPA-MOC-31 was the hepatic uptake and hepatobiliary excretion, which was associated with relatively unstable labeling of antibodies using heptadentate DTPA [53]. An interesting finding was that although

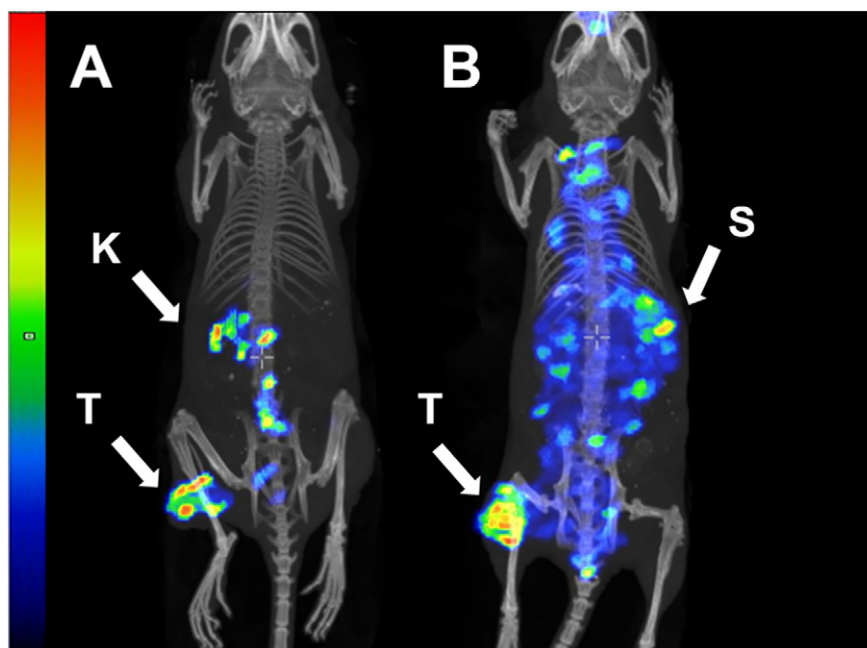


**Fig. 6.** SPECT/CT imaging of EpCAM-positive BxPC-3 xenografts at 6 h pi using: (A)  $^{125}\text{I}$ -PIB-H<sub>6</sub>-Ec1 and (B)  $^{125}\text{I}$ -H<sub>6</sub>-Ec1. Arrows indicate: T- tumor, K-kidneys, S- stomach.

expression of EpCAM has been documented in a number of tissues (e.g. gastrointestinal and respiratory tracts, thyroid) [54], the uptake of  $^{111}\text{In}$ -DTPA-MOC-31 in these tissues was quite low. For example, the activity in the abdomen was found in feces but not in the intestinal walls. The authors concluded that EpCAM in normal epithelia did not bind the imaging probe due to an intact basal membrane that forms a barrier against antibodies [53]. Similar observations have also been made for the  $^{99\text{m}}\text{Tc}$ -labeled F(ab)<sub>2</sub> fragment of the anti-EpCAM antibody 323/A3 [55] and the Fab fragment of the anti-EpCAM antibody nofetumomab (NR-LU-10) [56]. These findings suggest that imaging of EpCAM-expressing tumors and metastases in the abdomen is possible if an imaging probe has low hepatic uptake and hepatobiliary excretion.  $^{99\text{m}}\text{Tc}$ -labeled Fab nofetumomab merpentan has been approved by the FDA in 1998 (trade name Verluma) for the staging of lung cancer, gastrointestinal, breast, ovary, pancreas, kidney, cervix, and bladder carcinomas. However,  $^{18}\text{F}$ -FDG has outcompeted this imaging probe. In the murine model used herein,  $^{125}\text{I}$ -PIB-H<sub>6</sub>-Ec1 demonstrated appreciably lower uptake in the blood, lungs, liver, spleen, intestines and stomach at 3 h after injection compared to that of  $^{99\text{m}}\text{Tc}$ -Fab NR-LU-10 at 4 h after injection [57]. This resulted in noticeably higher tumor-to-organ ratios for  $^{125}\text{I}$ -PIB-H<sub>6</sub>-Ec1. Thus, PIB-H<sub>6</sub>-Ec1 could be utilized for imaging EpCAM expression using SPECT (with  $^{123}\text{I}$  as a label) and PET (using  $^{124}\text{I}$ ).

Prior to this study, several other formats of probes for imaging EpCAM have been evaluated in mice. The use of full-length IgGs provided peak uptake at 2–3 days after injection, and the tumor-to-blood ratio did not exceed five at that time point [58,59]. A  $^{99\text{m}}\text{Tc}$ -labeled anti-EpCAM 4D5MOC-B scFv provided tumor-to-blood ratios of 1.4 and 5.3 at 4 and 24 h after injection, respectively [60]. However, the tumor uptake was lower than the liver uptake at both time points [60]. In an interesting study performed by Eder and coworkers [43], a series of anti-EpCAM scFv42 derivatives (monomer, diabody, tribody and IgG) was constructed, labeled with  $^{68}\text{Ga}$  and evaluated in mice bearing HT-29 xenografts. The best variant, the diabody, had a tumor-to-blood ratio of 2, and the tumor-to-liver and tumor-to-lung ratios were between 1 and 2 at 3 h pi.  $^{89}\text{Zr}$ -labeled AMG 110, a bispecific T-cell engager antibody construct which targets EpCAM, is probably the best probe previously evaluated [44]. It provided tumor-to-blood ratios of approximately 35, 55 and 65 at 24, 72 and 144 h after injection, respectively. However, the tumor-to-liver ratio was not more than one. A comparison of  $^{125}\text{I}$ -PIB-H<sub>6</sub>-Ec1 with other EpCAM-imaging probes, evaluated in HT-29 model in earlier studies, demonstrated that  $^{125}\text{I}$ -PIB-H<sub>6</sub>-Ec1 provides the highest EpCAM imaging contrast on the day of injection in preclinical studies to date.

## 5. Conclusions

Selecting an optimal labeling strategy enables a substantial improvement in DARPIn-mediated imaging of expression of therapeutic molecular targets in vivo. This study confirmed that knowledge concerning one type of DARPIn can be generalized for other types. When a DARPIn-based probe is slowly internalized by cancer cells, the use of a non-residualizing label is preferable. Indirectly radioiodinated DARPIn H<sub>6</sub>-Ec1 provided high-contrast imaging of EpCAM-expressing xenografts a few hours after injection and is a promising tracer for imaging EpCAM expression in pancreatic cancer.

## CRedit authorship contribution statement

**Sergey M. Deyev:** Conceptualization, Investigation, Methodology, Supervision, Project administration, Funding acquisition, Writing - review & editing. **Anzhelika Vorobyeva:** Conceptualization, Investigation, Methodology, Data curation, Writing - original draft. **Alexey Schulga:** Investigation, Methodology, Funding acquisition, Writing - review & editing. **Ayman Abouzayed:** Investigation, Methodology, Formal analysis, Writing - review & editing. **Tyran Günther:** Investigation,

Methodology, Formal analysis, Writing - review & editing. **Javad Garousi:** Investigation, Methodology, Formal analysis, Writing - review & editing. **Elena Konovalova:** Investigation, Methodology, Formal analysis, Writing - review & editing. **Haozhong Ding:** Investigation, Methodology, Formal analysis, Writing - review & editing. **Torbjörn Gråslund:** Investigation, Methodology, Formal analysis, Writing - review & editing. **Anna Orlova:** Investigation, Methodology, Funding acquisition, Writing - review & editing, Formal analysis. **Vladimir Tolmachev:** Conceptualization, Methodology, Funding acquisition, Supervision, Project administration, Writing - review & editing.

## Declaration of competing interest

The authors have no competing interests to declare.

## Acknowledgments

This research was funded by the Swedish Cancer Society [CAN 2015/350 and 2017/425], Swedish Research Council [2015-02353 and 2015-02509], RSF [grant No. 19-14-00112] in the part of protein engineering and by the RFBR grants [18-04-00365 A, 18-29-08030 mk] in the part of protein purification and characterization. The molecular imaging work was supported by the Wallenberg infrastructure for PET-MRI (WIPPET) at the SciLifeLab Pilot Facility for Preclinical PET-MRI, Swedish nationally available imaging platform at Uppsala University, Sweden, financed by Knut and Alice Wallenberg Foundation (SPECT/CT).

## Appendix A. Supplementary data

Supplementary data to this article can be found online at <https://doi.org/10.1016/j.ijbiomac.2019.12.147>.

## References

- [1] I. Dagogo-Jack, A.T. Shaw, Tumour heterogeneity and resistance to cancer therapies, *Nat. Rev. Clin. Oncol.* 15 (2018) 81–94, <https://doi.org/10.1038/nrclinonc.2017.166>.
- [2] A.C. Wolff, M.E. Hammond, D.G. Hicks, M. Dowsett, L.M. McShane, K.H. Allison, D.C. Allred, J.M. Bartlett, M. Bilous, P. Fitzgibbons, W. Hanna, R.B. Jenkins, P.B. Mangu, S. Paik, E.A. Perez, M.F. Press, P.A. Spears, G.H. Vance, G. Viale, D.F. Hayes, American Society of Clinical Oncology, College of American Pathologists, Recommendations for human epidermal growth factor receptor 2 testing in breast cancer: American Society of Clinical Oncology/College of American Pathologists clinical practice guideline update, *J. Clin. Oncol.* 31 (2013) 3997–4013.
- [3] D.A. Mankoff, M.D. Farwell, A.S. Clark, D.A. Pryma, Making molecular imaging a clinical tool for precision oncology: a review, *JAMA Oncol* 3 (2017) 695–701, <https://doi.org/10.1001/jamaoncol.2016.5084>.
- [4] E.G.E. de Vries, L. Kist de Ruijter, M.N. Lub-de Hooge, R.A. Dierckx, S.G. Elias, S.F. Oosting, Integrating molecular nuclear imaging in clinical research to improve anti-cancer therapy, *Nat. Rev. Clin. Oncol.* 16 (2019) 241–255, <https://doi.org/10.1038/s41571-018-0123-y>.
- [5] G.A. Ulaner, S.K. Lyashchenko, C. Riedl, S. Ruan, P.B. Zanzonico, D. Lake, K. Jhaveri, B. Zeglis, J.S. Lewis, J.A. O'Donoghue, First-in-human human epidermal growth factor receptor 2-targeted imaging using  $^{89}\text{Zr}$ -pertuzumab PET/CT: dosimetry and clinical application in patients with breast cancer, *J. Nucl. Med.* 59 (2018) 900–906, <https://doi.org/10.2967/jnumed.117.202010>.
- [6] F. Bensch, L.E. Lamberts, M.M. Smeenk, A. Jorritsma-Smit, M.N. Lub-de Hooge, A.G.T. Terwisscha van Scheltinga, J.R. de Jong, J.A. Gietema, C.P. Schröder, M. Thomas, W. Jacob, K. Abiraj, C. Adessi, G. Meneses-Lorente, I. James, M. Weisser, A.H. Brouwers, E.G.E. de Vries,  $^{89}\text{Zr}$ -lumretuzumab PET imaging before and during HER3 antibody lumretuzumab treatment in patients with solid tumors, *Clin. Cancer Res.* 23 (2017) 6128–6137, <https://doi.org/10.1158/1078-0432.CCR-17-0311>.
- [7] Y.W. Jauw, J.M. Zijlstra, D. de Jong, D.J. Vugts, S. Zweegman, O.S. Hoekstra, G.A. van Dongen, M.C. Huisman, Performance of  $^{89}\text{Zr}$ -labeled-rituximab-PET as an imaging biomarker to assess CD20 targeting: a pilot study in patients with relapsed/refractory diffuse large B cell lymphoma, *PLoS One* 12 (2017), e0169828. <https://doi.org/10.1371/journal.pone.0169828>.
- [8] A. Krasniqi, M. D'Huyvetter, N. Devoogdt, F.Y. Frejd, J. Sörensen, A. Orlova, M. Keyaerts, V. Tolmachev, Same-day imaging using small proteins: clinical experience and translational prospects in oncology, *J. Nucl. Med.* 59 (2018) 885–891, <https://doi.org/10.2967/jnumed.117.199901>.
- [9] P.A. Nygren, A. Skerra, Binding proteins from alternative scaffolds, *J. Immunol. Methods* 290 (2004) 3–28, <https://doi.org/10.1016/j.jim.2004.04.006>.
- [10] C. Jost, A. Plückthun, Engineered proteins with desired specificity: DARPins, other alternative scaffolds and bispecific IgGs, *Curr. Opin. Struct. Biol.* 27 (2014) 102–112, <https://doi.org/10.1016/j.sbi.2014.05.011>.

- [11] P. Ernst, A. Plückthun, Advances in the design and engineering of peptide-binding repeat proteins, *Biol. Chem.* 398 (2017) 23–29, <https://doi.org/10.1515/hsz-2016-0233>.
- [12] R. Goldstein, J. Sosabowski, M. Livanos, J. Leyton, K. Vigor, G. Bhavsar, G. Nagy-Davidescu, M. Rashid, E. Miranda, J. Yeung, B. Tolner, A. Plückthun, S. Mather, T. Meyer, K. Chester, Development of the designed ankyrin repeat protein (DARPin) G3 for HER2 molecular imaging, *Eur. J. Nucl. Med. Mol. Imaging* 42 (2015) 288–301, <https://doi.org/10.1007/s00259-014-2940-2>.
- [13] A. Vorobyeva, O. Bragina, M. Altai, B. Mitran, A. Orlova, A. Shulga, G. Proshkina, V. Chernov, V. Tolmachev, S. Deyev, Comparative evaluation of radioiodinated and technetium-labeled DARPin 9\_29 for radionuclide molecular imaging of HER2 expression in malignant tumors, *Contrast Media Mol. Imaging*. 2018 (2018), 6930425, <https://doi.org/10.1155/2018/6930425>.
- [14] S. Deyev, A. Vorobyeva, A. Schulga, G. Proshkina, R. Güler, J. Löfblom, B. Mitran, J. Garousi, M. Altai, J. Buijs, V. Chernov, A. Orlova, V. Tolmachev, Comparative evaluation of two DARPin variants: effect of affinity, size, and label on tumor targeting properties, *Mol. Pharm.* 16 (2019) 995–1008, <https://doi.org/10.1021/acs.molpharmaceut.8b00922>.
- [15] A. Vorobyeva, A. Schulga, E. Konovalova, R. Güler, B. Mitran, J. Garousi, S. Rinne, J. Löfblom, A. Orlova, S. Deyev, V. Tolmachev, Comparison of tumor-targeting properties of directly and indirectly radioiodinated designed ankyrin repeat protein (DARPin) G3 variants for molecular imaging of HER2, *Int. J. Oncol.* 54 (2019) 1209–1220, <https://doi.org/10.3892/ijo.2019.4712>.
- [16] A. Vorobyeva, A. Schulga, E. Konovalova, R. Güler, J. Löfblom, M. Sandström, J. Garousi, V. Chernov, O. Bragina, A. Orlova, V. Tolmachev, S. Deyev, Optimal composition and position of histidine-containing tags improves biodistribution of 99mTc-labeled DARPins, *Sci. Rep.* 9 (2019) 9405, <https://doi.org/10.1038/s41598-019-45795-8>.
- [17] F. Bensch, M.M. Smeenk, S.C. van Es, J.R. de Jong, C.P. Schröder, S.F. Oosting, M.N. Lub-de Hooge, C.W. Menke-van der Houven van Oordt, A.H. Brouwers, R. Boellaard, E.G.E. de Vries, Comparative biodistribution analysis across four different 89Zr-monooclonal antibody tracers—the first step towards an imaging warehouse, *Theranostics* 8 (2018) 4295–4304, <https://doi.org/10.7150/thno.26370>.
- [18] F.B. van Gog, G.W. Visser, J.W. Stroomer, J.C. Roos, G.B. Snow, G.A. van Dongen, High dose rhenium-186-labeling of monoclonal antibodies for clinical application: pitfalls and solutions, *Cancer* 80 (1997) 2360–2370.
- [19] E.W. Price, K.E. Carnazza, S.D. Carlin, A. Cho, K.J. Edwards, K.K. Sevak, J.M. Glaser, E. de Stanchina, Y.Y. Janjigian, J.S. Lewis, 89Zr-DFO-AMG102 immuno-PET to determine local hepatocyte growth factor protein levels in tumors for enhanced patient selection, *J. Nucl. Med.* 58 (2017) 1386–1394, <https://doi.org/10.2967/jnumed.116.187310>.
- [20] V. Tolmachev, A. Orlova, Influence of labelling methods on biodistribution and imaging properties of radiolabelled peptides for visualisation of molecular therapeutic targets, *Curr. Med. Chem.* 17 (2010) 2636–2655, <https://doi.org/10.2174/092986710791859397>.
- [21] A. Vorobyeva, A. Schulga, S.S. Rinne, T. Günther, A. Orlova, S. Deyev, V. Tolmachev, Indirect radioiodination of DARPin G3 using N-succinimidyl-para-iodobenzoate improves the contrast of HER2 molecular imaging, *Int. J. Mol. Sci.* 20 (2019) <https://doi.org/10.3390/ijms20123047pii>: E3047.
- [22] N. Stefan, P. Martin-Killias, S. Wyss-Stoekle, A. Honegger, U. Zangemeister-Wittke, A. Plückthun, DARPins recognizing the tumor-associated antigen EpCAM selected by phage and ribosome display and engineered for multivalency, *J. Mol. Biol.* 413 (2011) 826–843, <https://doi.org/10.1016/j.jmb.2011.09.016>.
- [23] S. Eyvazi, S. Farajnia, S. Dastmalchi, F. Kanipour, H. Zarredar, M. Bandehpour, Antibody based EpCAM targeted therapy of cancer, review and update, *Cancer Drug Targets* 18 (2018) 857–868, <https://doi.org/10.2174/1568009618666180102102311>.
- [24] N. Brychta, M. Drosch, C. Driemel, J.C. Fischer, R.P. Neves, I. Esposito, W. Knoefel, B. Möhlendick, C. Hille, A. Stresemann, T. Krahn, M.U. Kassack, N.H. Stoeklein, O. von Ahnsen, Isolation of circulating tumor cells from pancreatic cancer by automated filtration, *Oncotarget* 8 (2017) 86143–86156, <https://doi.org/10.18632/oncotarget.21026>.
- [25] M. Ducreux, A.S. Cuhna, C. Caramella, A. Hollebecque, P. Burtin, D. Goéré, T. Seufferlein, K. Haustermans, J.L. Van Laethem, T. Conroy, D. Arnold, ESMO Guidelines Committee, cancer of the pancreas: ESMO clinical practice guidelines for diagnosis, treatment and follow-up, *Ann. Oncol.* 26 (2015) v56–v68, <https://doi.org/10.1093/annonc/mdv295>.
- [26] I.T. Konstantinidis, A.L. Warshaw, J.N. Allen, L.S. Blaszkowsky, C.F. Castillo, V. Deshpande, T.S. Hong, E.L. Kwak, G.Y. Lauwers, D.P. Ryan, J.A. Wargo, K.D. Lillemoe, C.R. Ferrone, Pancreatic ductal adenocarcinoma: is there a survival difference for R1 resections versus locally advanced unresectable tumors? What is a “true” R0 resection? *Ann. Surg.* 257 (2013) 731–736, <https://doi.org/10.1097/SLA.0b013e318263da2f>.
- [27] D. Fong, M. Steurer, P. Obrist, V. Barbieri, R. Margreiter, A. Amberger, K. Laimer, G. Gastl, A. Tzankov, G. Spizzo, Ep-CAM expression in pancreatic and ampullary carcinomas: frequency and prognostic relevance, *J. Clin. Pathol.* 61 (2008) 31–35, <https://doi.org/10.1136/jcp.2006.037333>.
- [28] G. Spizzo, D. Fong, M. Wurm, C. Ensinger, P. Obrist, C. Hofer, G. Mazzoleni, G. Gastl, P. Went, EpCAM expression in primary tumour tissues and metastases: an immunohistochemical analysis, *J. Clin. Pathol.* 64 (2011) 415–420, <https://doi.org/10.1136/jcp.2011.090274>.
- [29] C. Li, D.G. Heidt, P. Dalerba, C.F. Burant, L. Zhang, V. Adsay, M. Wicha, M.F. Clarke, D.M. Simeone, Identification of pancreatic cancer stem cells, *Cancer Res.* 67 (2007) 1030–1037, <https://doi.org/10.1158/0008-5472.CAN-06-2030>.
- [30] M. Schmidt, M.E. Scheulen, C. Dittrich, P. Obrist, N. Marschner, L. Dirix, M. Schmidt, D. Rüttinger, M. Schuler, C. Reinhardt, A. Awada, An open-label, randomized phase II study of adecatumumab, a fully human anti-EpCAM antibody, as monotherapy in patients with metastatic breast cancer, *Ann. Oncol.* 21 (2010) 275–282, <https://doi.org/10.1093/annonc/mdp314>.
- [31] R. Waibel, R. Alberto, J. Willuda, R. Finner, R. Schibli, A. Stichelberger, A. Egli, U. Abram, J.P. Mach, A. Plückthun, P.A. Schubiger, Stable one-step technetium-99m labeling of his-tagged recombinant proteins with a novel Tc(1)-carbonyl complex, *Nat. Biotechnol.* 17 (1999) 897–901, <https://doi.org/10.1038/12890>.
- [32] I. Vaneycken, N. Devoogdt, N. Van Gassen, C. Vincke, C. Xavier, U. Wernery, S. Muyllderms, T. Lahoutte, V. Cavelliers, Preclinical screening of anti-HER2 nanobodies for molecular imaging of breast cancer, *FASEB J.* 25 (2011) 2433–2446, <https://doi.org/10.1096/fj.10-180331>.
- [33] A. Ku, C. Chan, S. Aghevlian, Z. Cai, D. Cescon, S.V. Bratman, L. Ailles, D.W. Hedley, R.M. Reilly, MicroSPECT/CT imaging of cell-line and patient-derived EGFR-positive tumor xenografts in mice with panitumumab fab modified with hexahistidine peptides to enable labeling with 99mTc(1) tricarbonyl complex, *Mol. Pharm.* 16 (2019) 3559–3568, <https://doi.org/10.1021/acs.molpharmaceut.9b00422>.
- [34] C. Hofstrom, A. Orlova, M. Altai, F. Wangsell, T. Graslund, V. Tolmachev, Use of a HEHEHE purification tag instead of a hexahistidine tag improves biodistribution of affibody molecules site-specifically labeled with (99m)Tc, (111)In, and (125)I, *J. Med. Chem.* 54 (2011) 3817–3826, <https://doi.org/10.1021/jm200065e>.
- [35] A. Orlova, C. Hofström, J. Strand, Z. Varasteh, M. Sandström, K. Andersson, V. Tolmachev, T. Gräslund, [99mTc(CO)3]+-(HE)3-ZIGF1R:4551, a new Affibody conjugate for visualization of insulin-like growth factor-1 receptor expression in malignant tumours, *Eur. J. Nucl. Med. Mol. Imaging* 40 (2013) 439–449, <https://doi.org/10.1007/s00259-012-2284-8>.
- [36] J. Garousi, H. Honarvar, K.G. Andersson, B. Mitran, A. Orlova, J. Buijs, J. Löfblom, F.Y. Frejd, V. Tolmachev, Comparative evaluation of affibody molecules for radionuclide imaging of in vivo expression of carbonic anhydrase IX, *Mol. Pharm.* 13 (2016) 3676–3687, <https://doi.org/10.1021/acs.molpharmaceut.6b00502>.
- [37] D.S. Wilbur, S.W. Hadley, L.M. Grant, M.D. Hylarides, Radiiodinated iodobenzoyl conjugates of a monoclonal antibody Fab fragment. In vivo comparisons with chloramine-T-labeled Fab, *Bioconjug. Chem.* 2 (1991) 111–116.
- [38] M. Pruszynski, E. Koumariou, G. Vaidyanathan, H. Revets, N. Devoogdt, T. Lahoutte, H.K. Lyerly, M.R. Zalutsky, Improved tumor targeting of anti-HER2 nanobody through N-succinimidyl 4-guanidinomethyl-3-iodobenzoate radiolabeling, *J. Nucl. Med.* 55 (2014) 650–656, <https://doi.org/10.2967/jnumed.113.127100>.
- [39] A.C. Steffen, M. Wikman, V. Tolmachev, G.P. Adams, F.Y. Nilsson, S. Ståhl, J. Carlsson, In vitro characterization of a bivalent anti-HER-2 affibody with potential for radionuclide-based diagnostics, *Cancer Biother. Radiopharm.* 20 (2005) 239–248, <https://doi.org/10.1089/cbr.2005.20.239>.
- [40] H. Wällberg, A. Orlova, Slow internalization of anti-HER2 synthetic affibody monomer 111In-DOTA-ZHER2:342-pep2: implications for development of labeled tracers, *Cancer Biother. Radiopharm.* 23 (2008) 435–442, <https://doi.org/10.1089/cbr.2008.0464>.
- [41] V. Tolmachev, A. Orlova, K. Andersson, Methods for radiolabelling of monoclonal antibodies, *Methods Mol. Biol.* 1060 (2014) 309–330, [https://doi.org/10.1007/978-1-62703-586-6\\_16](https://doi.org/10.1007/978-1-62703-586-6_16).
- [42] Y. Meng, B.Q. Xu, Z.G. Fu, B. Wu, B. Xu, Z.N. Chen, L. Li, Cytoplasmic EpCAM overexpression is associated with favorable clinical outcomes in pancreatic cancer patients with hepatitis B virus negative infection, *Int. J. Clin. Exp. Med.* 8 (2015) 22204–22216.
- [43] M. Eder, S. Knackmuss, F. Le Gall, U. Reusch, V. Rybin, M. Little, U. Haberkorn, W. Mier, M. Eisenhut, 68Ga-labelled recombinant antibody variants for immuno-PET imaging of solid tumours, *Eur. J. Nucl. Med. Mol. Imaging* 37 (2010) 1397–1407, <https://doi.org/10.1007/s00259-010-1392-6>.
- [44] F.J. Warders, S.J. Waaij, M. Pool, M.N. Lub-de Hooge, M. Friedrich, A.G. Terwisscha van Scheltinga, P. Deegen, S.K. Stienens, P.C. Pieslor, H.K. Cheung, J.G. Kosterink, E.G. de Vries, Biodistribution and PET imaging of labeled bispecific T cell-engaging antibody targeting EpCAM, *J. Nucl. Med.* 57 (2016) 812–817, <https://doi.org/10.2967/jnumed.115.168153>.
- [45] K.R. Hess, G.R. Varadhachary, S.H. Taylor, W. Wei, M.N. Raber, R. Lenzi, J.L. Abbruzzese, Metastatic patterns in adenocarcinoma, *Cancer* 106 (2006) 1624–1633, <https://doi.org/10.1002/cncr.21778>.
- [46] V. Tolmachev, C. Hofström, J. Malmberg, S. Ahlgren, S.J. Hosseinimehr, M. Sandström, L. Abrahmsén, A. Orlova, T. Gräslund, HEHEHE-tagged affibody molecule may be purified by IMAC, is conveniently labeled with [99m]Tc(CO)3(+), and shows improved biodistribution with reduced hepatic radioactivity accumulation, *Bioconjug. Chem.* 21 (2010) 2013–2022, <https://doi.org/10.1021/bc1002357>.
- [47] C. Hofström, M. Altai, H. Honarvar, J. Strand, J. Malmberg, S.J. Hosseinimehr, A. Orlova, T. Gräslund, V. Tolmachev, HAHAAA, HEHEHE, HHHHHL, or HKHKHK: influence of position and composition of histidine containing tags on biodistribution of [(99m)Tc(CO)3](+)-labeled affibody molecules, *J. Med. Chem.* 56 (2013) 4966–4974, <https://doi.org/10.1021/jm400218y>.
- [48] S. Lindbo, J. Garousi, M. Åstrand, H. Honarvar, A. Orlova, S. Hober, V. Tolmachev, Influence of histidine-containing tags on the biodistribution of ADAPT scaffold proteins, *Bioconjug. Chem.* 27 (2016) 716–726, <https://doi.org/10.1021/acs.bioconjugchem.5b00677>.
- [49] T. Kamisawa, T. Isawa, M. Koike, K. Tsuruta, A. Okamoto, Hematogenous metastases of pancreatic ductal carcinoma, *Pancreas* 11 (1995) 345–349.
- [50] C. Decristoforo, L. Melendez-Alafort, J.K. Sosabowski, S.J. Mather, 99mTc-HYNIC-[Tyr3]-octreotide for imaging somatostatin-receptor-positive tumors: preclinical evaluation and comparison with 111In-octreotide, *J. Nucl. Med.* 41 (2000) 1114–1119.
- [51] A. Schmitt, P. Bernhardt, O. Nilsson, H. Ahlman, L. Kölbj, E. Forssell-Aronsson, Differences in biodistribution between 99mTc-depreotide, 111In-DTPA-octreotide, and

- 177Lu-DOTA-Tyr3-octreotate in a small cell lung cancer animal model, *Cancer Biother. Radiopharm.* 20 (2005) 231–236.
- [52] N. Oshima, H. Akizawa, S. Zhao, Y. Zhao, K. Nishijima, Y. Kitamura, Y. Arano, Y. Kuge, K. Ohkura, Design, synthesis and biological evaluation of negatively charged <sup>111</sup>In-DTPA-octreotide derivatives, *Bioorg. Med. Chem.* 22 (2014) 1377–1382, <https://doi.org/10.1016/j.bmc.2013.12.063>.
- [53] J.G. Kosterink, M.W. de Jonge, E.F. Smit, D.A. Piers, R.A. Kengen, P.E. Postmus, D. Shochat, H.J. Groen, H.T. The, L. de Leij, Pharmacokinetics and scintigraphy of indium-111-DTPA-MOC-31 in small-cell lung carcinoma, *J. Nucl. Med.* 36 (1995) 2356–2362.
- [54] M. Balzar, M.J. Winter, C.J. de Boer, S.V. Litvinov, The biology of the 17-1A antigen (Ep-CAM), *J. Mol. Med. (Berl)*. 77 (1999) 699–712.
- [55] R. De Bree, J.C. Roos, J.J. Quak, W. Den Hollander, G.B. Snow, G.A. Van Dongen, Clinical screening of monoclonal antibodies 323/A3, cSF-25 and K928 for suitability of targeting tumours in the upper aerodigestive and respiratory tract, *Nucl. Med. Commun.* 15 (1994) 613–627, <https://doi.org/10.1097/00006231-199408000-00006>.
- [56] H.B. Breitz, A. Tyler, M.J. Bjorn, T. Lesley, P.L. Weiden, Clinical experience with Tc-99m nofetumomab merpentan (Verluma) radioimmunosintigraphy, *Clin. Nucl. Med.* 22 (1997) 615–620, <https://doi.org/10.1097/00003072-199709000-00007>.
- [57] S. Kasina, J.A. Sanderson, J.N. Fitzner, A. Srinivasan, T.N. Rao, L.J. Hobson, J.M. Reno, D.B. Axworthy, P.L. Beaumier, A.R. Fritzberg, Simplified preformed chelate protein radiolabeling with technetium-99m mercaptoacetamidoadipoylglycylglycine (N3S-adipate), *Bioconjug. Chem.* 9 (1998) 108–117, <https://doi.org/10.1021/bc970047i>.
- [58] E. Kievit, F.B. van Gog, H.M. Schlüper, G.A. van Dongen, H.M. Pinedo, E. Boven, Comparison of the biodistribution and the efficacy of monoclonal antibody 323/A3 labeled with either <sup>131</sup>I or <sup>186</sup>Re in human ovarian cancer xenografts, *Int. J. Radiat. Oncol. Biol. Phys.* 38 (1997) 813–823, [https://doi.org/10.1016/s0360-3016\(97\)00007-2](https://doi.org/10.1016/s0360-3016(97)00007-2).
- [59] S.C. Ghosh, K.L. Pinkston, H. Robinson, B.R. Harvey, N. Wilganowski, K. Gore, E.M. Sevick-Muraca, A. Azhdarinia, Comparison of DOTA and NODAGA as chelators for (64)cu-labeled immunoconjugates, *Nucl. Med. Biol.* 42 (2015) 177–183, <https://doi.org/10.1016/j.nucmedbio.2014.09.009>.
- [60] J. Willuda, A. Honegger, R. Waibel, P.A. Schubiger, R. Stahel, U. Zangemeister-Wittke, A. Plückthun, High thermal stability is essential for tumor targeting of antibody fragments: engineering of a humanized anti-epithelial glycoprotein-2 (epithelial cell adhesion molecule) single-chain Fv fragment, *Cancer Res.* 59 (1999) 5758–5777.